Effect of low Zn doping on the Verwey transition in magnetite single crystals: Mössbauer spectroscopy and x-ray diffraction

V. Chlan,[1] J. Żukrowski,[2] A. Bosak,[3] Z. Kąkol,[4] A. Kozłowski,[4] Z. Tarnawski,[4] R. Řezníček,[1,5] H. Štěpánková,[1] P. Novák,[6] I. Biało,[4] and J. M. Honig[7]

[1]*Faculty of Mathematics and Physics, Charles University, V Holešovičkách 2, 180 00 Prague 8, Czech Republic*
[2]*Academic Center of Materials and Nanotechnology, AGH University of Science and Technology, al. Mickiewicza 30, 30-059 Kraków, Poland*
[3]*European Synchrotron Radiation Facility, 6 rue Jules Horowitz, F-38043 Grenoble Cedex, France*
[4]*Faculty of Physics and Applied Computer Science, AGH University of Science and Technology, al. Mickiewicza 30, 30-059 Kraków, Poland*
[5]*Faculty of Physics and Earth Sciences, University of Leipzig, Linnéstrasse 5, D-04103 Leipzig, Germany*
[6]*Institute of Physics of ASCR, Cukrovarnická 10, 162 53 Prague 6, Czech Republic*
[7]*Department of Chemistry, Purdue University, West Lafayette, Indiana 47907-2084, USA*

(Received 8 May 2018; revised manuscript received 8 August 2018; published 24 September 2018)

To observe, by microscopic probe, how low Zn doping in $Fe_{3-x}Zn_xO_4$ (x is below 1%) changes the Verwey transition, we have performed Mössbauer spectroscopy measurements on three single crystalline samples with various Zn doping. In spectra analysis we used the recently published model of Mössbauer data treatment formulated as a result of *ab initio* calculations for a low-temperature monoclinic structure (of *Cc* symmetry) of magnetite. It was suggested there that the hyperfine parameters for all 24 Fe distinct positions in the lattice can be grouped into four major components with very similar hyperfine parameters within each set. Using these parameters as starting values, very good fits were obtained for magnetite with low doping level, while for higher doping, $x = 0.03$, where the Verwey transition changes its character, one component is significantly different. In particular, low hyperfine field $B_{\text{eff}} = 36\,\text{T}$, considered as a characteristic feature of the *Cc* phase spectrum, is absent here. Also, in this case, the high-temperature spectra are different from those for lower doped magnetite showing more pronounced continuous alteration with temperature. This might be due to crystal structure of lower than *Fd-3m* symmetry, a fact suggested by our x-ray synchrotron studies. All this triggered a discussion about an experimental fingerprint for the difference between these two classes of magnetite, frequently referred to as magnetite of first- and second-order Verwey transition, and about the electronic structure of both kinds of systems.

DOI: 10.1103/PhysRevB.98.125138

I. INTRODUCTION

Magnetite became a model material for solid-state physics because competing interactions are present there, resulting in both a ferrimagnetic to paramagnetic phase transition at $T_C = 858\,\text{K}$ and the semiconductor to semimetal Verwey transition when T exceeds $T_V = 125\,\text{K}$ [1]. Despite the presence of just two elements, magnetite properties are very rich and complicated: the low-T structure was only recently solved [2], and a concise description of magnetite properties and the relationship between them is still lacking.

At $T > 125$ K, stoichiometric magnetite has cubic *Fd-3m* symmetry. The unit cell consists of 56 atoms, of which 32 are oxygen atoms forming octahedral (B) and tetrahedral (A) voids, with 24 Fe atoms (ions) residing in those voids. In tetrahedral voids, Fe atoms are in a +3 state that does not seem to change appreciably when T lowers below T_V, while in B positions the mean valence is +2.5. The low-T structure is monoclinic *Cc* [2], with the unit cell four times bigger than cubic, doubled in the c direction, and with Fe residing in 16 B inequivalent positions and 8 A inequivalent positions. Iron B atoms, with noninteger valences, are grouped in cigarlike arrangements, dubbed trimerons [2], with each trimeron consisting roughly of one 2+-like ion in the center and two 3+-like ions at the ends. Although this trimeron structure was questioned [3], it was supported by structural measurements [2], NMR [4], and Mössbauer [5] experiments in conjunction with *in situ* density functional theory (DFT) calculations. Indeed, NMR and Mössbauer calculated spectra, with the structure from [2] imposed, were able to reproduce experimental data much better than in [3]. Thus, the trimeron structure seems to be well established at least for stoichiometric magnetite.

Among many spectacular phenomena related to magnetite, the change of the Verwey transition character from discontinuous (with a latent heat but without appreciable hysteresis) to a wide, continuous transition [6] was not considered very often. The transfer from a "first-" to a "second-order" transition can be achieved either by nonstoichiometry, as in $Fe_{3(1-\delta)}O_4$, or by doping, as in $Fe_{3-x}M_xO_4$ ($x = \text{Ti}, \text{Zn}$), in case $3\delta = x$ exceeds 0.012. This universal $x = 3\delta$ relation, shown here in the case of T_V versus $x = 3\delta$ in Fig. 1S of the supplemental material [8], but observed in many other properties, is valid despite the fact that iron deficiency results in a change of Fe valence on octahedral positions, Ti enters octahedral positions giving four electrons to the system, and Zn replaces iron in tetrahedral sites with only two electrons yielded. Neither this universal behavior nor the fact that it is not reproduced for other elements was really explained.

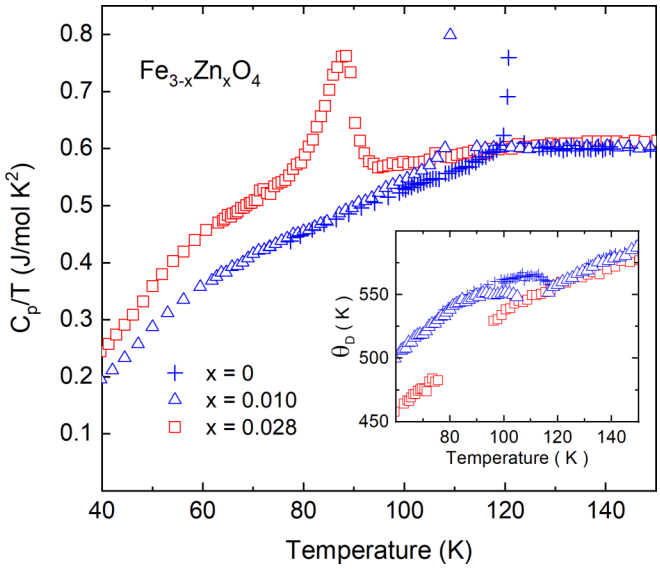

FIG. 1. Temperature dependence of the heat capacity of Zn-doped magnetite single crystals typical for both regimes of Verwey transition order (based on [12]). Heat-capacity baselines for first-order samples lie below those for second order, a fact that is quantified in the inset as the temperature dependence of Debye's temperature (θ_D in the transition region was removed for clarity). Note that a comparable difference in θ_D is maintained down to 0.3 K [10] and that the difference in baselines is linked to electronic effects, not lattice vibrations [12].

Samples with first- and second-order transitions are particularly well distinguished from each other when the heat capacity at $T < T_V$ is considered. In the case of first-order magnetite, the baseline of heat capacity lies considerably below the baseline for second-order materials, Fig. 1, and this difference persists down to the lowest temperatures (0.3 K) [10,11]. Although quantified here as different Debye temperature, this difference is probably linked to electronic states rather than lattice vibrations [12], but changes in the atomic arrangements, e.g., some disorder in the trimeron structure, certainly play a role.

With these facts in mind, we tried to find a microscopic difference between first- and second-order magnetite using Mössbauer spectroscopy and making use of a recently calculated electronic structure of the low-T Cc phase of magnetite and the prediction of hyperfine (HF) parameters calculated in [5]. Although calculations were made only for stoichiometric magnetite, we applied these parameters here to two Zn-doped magnetite single crystals with different order Verwey transition, implicitly assuming the same trimeron-like Cc symmetry for magnetite of both orders. For completeness, the results for the stoichiometric magnetite crystal, the same as shown in [5], were also shown. Mössbauer spectroscopy results were supplemented with structural synchrotron studies performed on nonstoichiometric single crystal.

II. EXPERIMENT

Mössbauer absorption was measured in three single crystalline magnetite samples, $Fe_{3-x}Zn_xO_4$, $x = 0$, 0.005, and 0.03, all grown in an identical way by the skull melting method [13]. After growing, the samples were annealed in a CO/CO_2 atmosphere in order to achieve stoichiometry [14,15]. The quality of the samples was checked by AC magnetic susceptibility χ_{AC} (and the results are shown in Fig. 2S of the supplemental material). Stoichiometric magnetite was the same as described in [5] and is presented here for completeness but also due to the fact that the fitting procedure used here was slightly different and the results at $T > T_V$ are also documented.

Measurement temperatures, Verwey transition temperatures, and the transition widths are shown in Table I. Here also the sample $3\delta = 0.0162$, where diffraction (at room temperature) was measured, is included.

The Mössbauer effect was measured in transmission in single crystalline samples oriented with the [001] axis (in cubic notation) parallel to γ-ray. Experimental details are described in the supplemental material [8], where also selected spectra are shown in Fig. 3S.

The results were processed in the following way: four components were fitted at $T < T_V$ with the starting hyperfine parameters for the fit drawn from DFT calculations in [5]. Three components were used in the fitting procedure at $T > T_V$: an A component and two B components. This is because at $T_{IP} = 130$ K (for $x = 0$) the system undergoes a $\langle 100\rangle \rightarrow \langle 111\rangle$ spin reorientation transition that leads to the splitting of the Fe(B) components into two with an ideal intensity ratio 1 (lower B_{eff}):3 (higher B_{eff}).

The fitting procedure worked well for first-order samples, while for the second-order samples more spectrum components gave better results. A more elaborate discussion about the fitting procedure will be presented below.

The fitted spectra for the lowest and highest temperatures are shown in Fig. 2, and the results in the form of the temperature dependence of hyperfine parameters are shown in Fig. 3 [17]. The details will be discussed below.

A few facts are noteworthy:

(i) There is a drastic change of the spectra while T drops below T_V, a fact found already in numerous Mössbauer spectroscopy results of magnetite. This change is due to both the

TABLE I. Verwey transition characterization and the temperatures of experiments (Mössbauer experiment and diffraction).

Sample	$T > T_V$ (K)	$T < T_V$ (K)	T_V (K)	ΔT_V (K)
$x = 0$	135, 140, 145, 150, 155, 160, 295	4.2, 25, 118, 121, 122	124.3	0.5
$x = 0.005$	160, 295	4.2, 72, 80, 100	116.9	2.9
$x = 0.03$	110,120,130,140,150,160,170,180,295	4.2, 72	86.5	6.1
$3\delta = 0.0162$	295		104.1	4.3

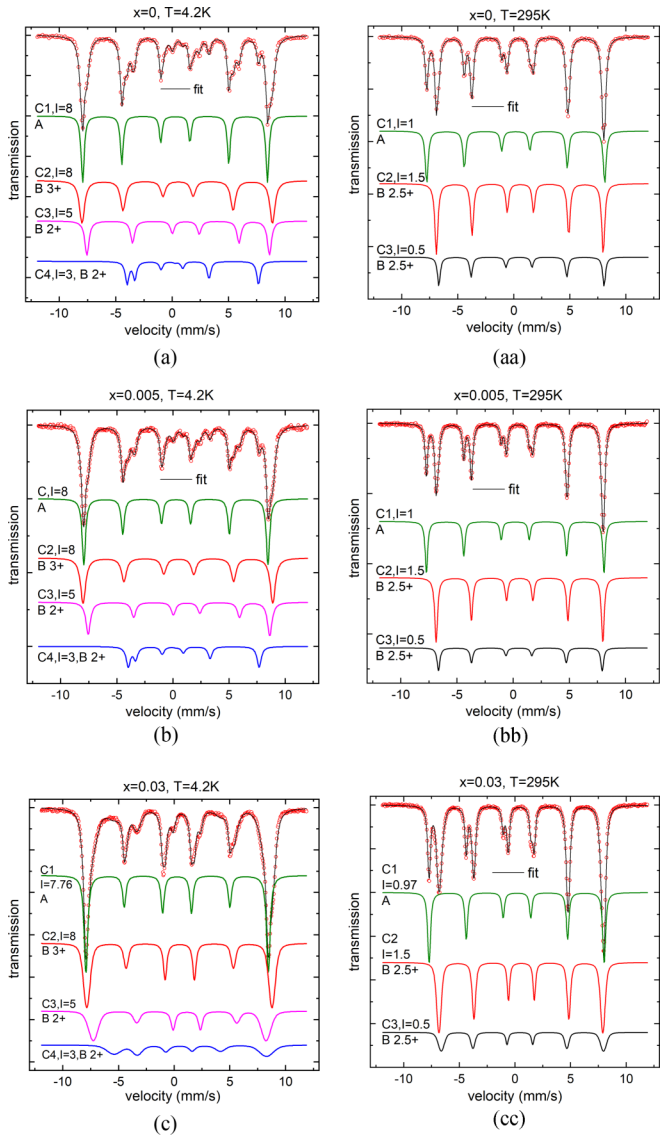

FIG. 2. (a) ($x = 0$), (b) ($x = 0.005$), and (c) ($x = 0.03$) experimental spectra (open circles) at $T = 4.2$ K with fits (black line) broken into components Ci identified by the site approximate valence and intensity (that sum up to the number of inequivalent Fe positions, 24 for stoichiometric magnetite). Each component is shifted to allow for better separation; the scale for each component is identical. Note that for $x = 0.03$, the line intensities for each component are not 3:2:1 as they are for other samples. (aa), (bb), and (cc). Experimental spectra (open circles) at $T = 295$ K with fits (black line) broken into components Ci identified by the site, approximate valence, and intensity (that sum up to 3 for stoichiometric magnetite).

change of symmetry and electronic structure, and it is not easy to separate these two effects.

(ii) There is a steady temperature variation of Mössbauer spectra for $x = 0.03$, both at $T > T_V$ and below T_V [Fig. 3S(c)]. Part of it is reflected in the temperature variation of the hyperfine parameters, but the change is even more pronounced for the line intensities.

(iii) This difference between first- and second-order samples is reflected in their effective field. B_{eff} for first-order samples breaks into well-defined parts: a high field, close to 50 T, and a low field, ~36 T [Figs. 2(a), 2(b), and 3]. In the case of $x = 0.03$, this division is no longer obvious. For this reason, the additional procedure was applied for all samples. Here the spectra were analyzed in terms of a Voigt-function-based magnetic splitting distribution [18,19]. The spectra were assumed to be a sum of four components with Gaussian hyperfine field distributions. The results of this analysis are presented in Fig. 4, and it is again clear that the low-field component for the $x = 0.03$ sample is nearly missing.

(iv) The shape of the spectra shown in Fig. 3S shows that the outermost lines, those of the highest B_{eff}, are to a large extent unaltered while the temperature is lowered. This general impression is supported by the temperature dependence of the hyperfine parameters shown in Fig. 3: they go smoothly across T_V to the low-T region, strongly suggesting that these parameters are for tetrahedral Fe^{3+} iron positions. Since the formal valence of these A positions is 3+, it allows us to attribute IS in these positions to 3+.

All these issues will be discussed below.

An x-ray synchrotron experiment was performed on the diffraction side station of the ID28 ESRF beamline (Grenoble, France) on nonstoichiometric crystal, $3\delta = 0.0162$, grown and annealed in an identical way as other samples; $\chi_{AC}(T)$ is presented in Fig. 2S of the supplemental material. The sample, a needlelike crystal with a cross section of 50 μm etched with hot concentrated HCl to remove the damaged surface layer, was prepared by cutting and polishing from a bigger crystal.

The diffraction side station of ID28 was equipped with a hybrid pixel PILATUS3 × 1M detector. Data collection at wavelength 0.6968 Å was performed with the angular step 0.1°, taking the full rotation needle axis. Data reduction was performed with the CRYSALIS (RIGAKU) software package [20]. High-resolution reciprocal space cuts were constructed using locally developed software. The results are presented and discussed below.

III. DISCUSSION

The main aim of our Mössbauer experiments was to observe the differences in local electronic arrangements in first- and second-order samples both in low- and high-temperature ranges.

A. $T < T_V$

To better understand the low-temperature spectra and to simplify the data analysis, we used the recipe from [5] of the data processing and a possible range of hyperfine parameters. In that paper, DFT calculations were performed for the ground state of magnetite, and hyperfine parameters were calculated for each of 24 nonequivalent Fe positions. Since no Mössbauer experiment can detect the subtle differences that exist between those 24 sets of hyperfine parameters, it was suggested to break all sites into four groups, each having very similar hyperfine parameters B_{eff} and IS, but slightly wider scatter of V_{zz}. Mean values of HF parameters of the Fe positions belonging to these groups were proposed as the starting values for the spectra refinement, and the simulated spectra with those parameters reproduced very well the experimental line positions and all the subtleties of the experimental

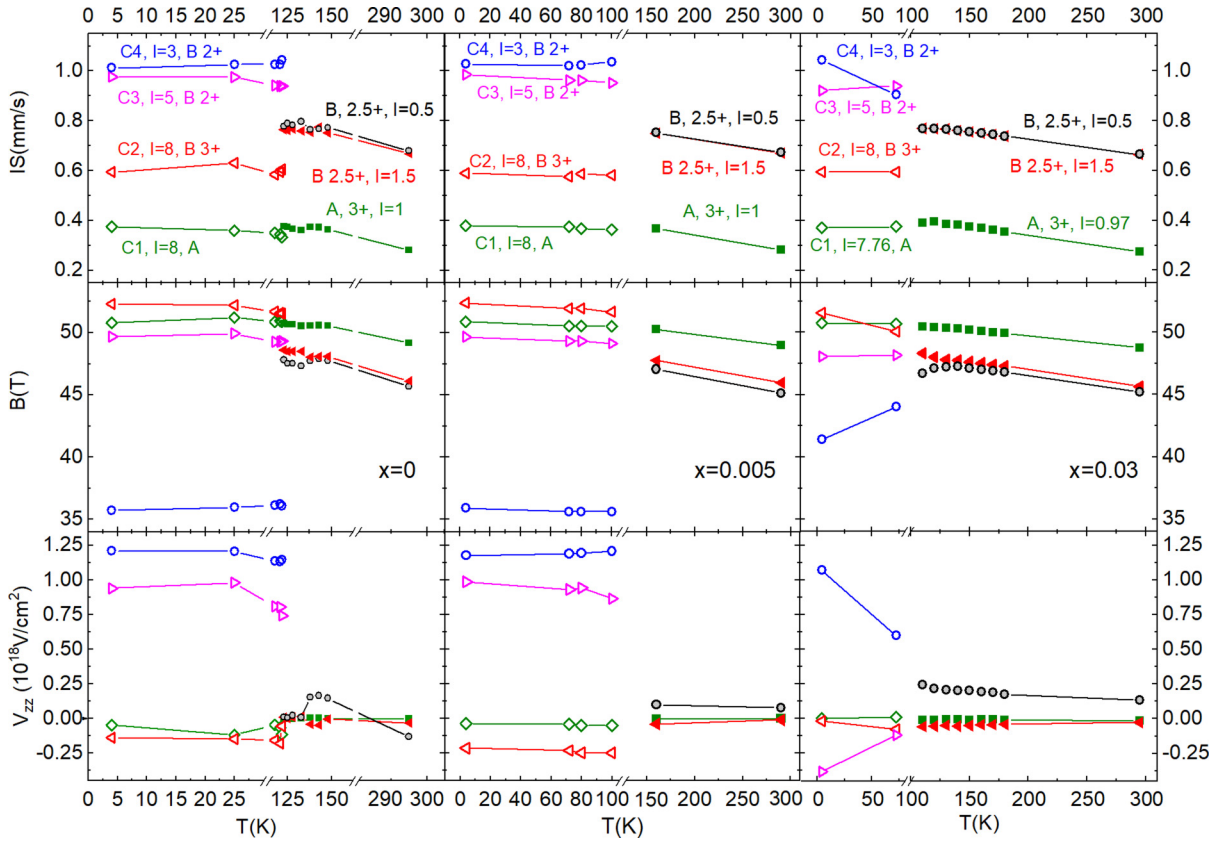

FIG. 3. Temperature dependence of hyperfine parameters. They are similar for stoichiometric and low-doped magnetite (two left panels) but different for $x = 0.03$, especially for B_{eff} and electric field gradient V_{zz}. Barely any change of hyperfine parameters of Fe A atoms is seen both at T_V and with doping.

Mössbauer spectrum. Although some corrections to the proposed initial values were needed to perfectly match the experiment (very small in the case of B_{eff} and IS, and higher for V_{zz}), it was proven that no experimental feature in the Mössbauer spectrum of stoichiometric magnetite exists that could not be understood by the electronic structure of magnetite calculated by DFT with the crystal structure proposed by Senn [2].

Bearing in mind very small Zn concentration as for our doped samples, we used, for $T < T_V$, the same model (four components) and the same suggested sets of hyperfine parameters as in [5]. The fitting uncertainties for $x = 0$ and 0.005 were small and similar, and both spectra give similar fitted HF parameters. In particular, one component is represented by very low B_{eff} (close to 36 T), the lowest valence (highest IS), and the largest V_{zz}, with all of these parameters suggesting a $3d$ electronic state close to asymmetric 2+. Such low-field values and high V_{zz} are well understood within DFT calculations [5]. Namely, the effective magnetic field acting on nuclear spin is composed of an isotropic Fermi contact term due to magnetically polarized s electrons entering the nucleus and an anisotropic term caused by dipolar interactions with electronic spins and orbital moments as well as a dipolar magnetic field from other ions. Usually the Fermi contact term dominates, but in magnetite the anisotropic parts are relatively high (>9 T) for component C3 (composed of positions B4, B14, B3, B2, and B1, according to the labeling in [5]) and especially for component C4 (B7, B13, and B16), while at the same time the isotropic component is relatively low (in the range 41–45 T). Since B_{eff} depends, via this anisotropic term tensor, on the magnetization direction (assumed to point along the c direction), it results in low $B_{\text{eff}} = 36$ T for B7, B13, and B16 (component C4), but not for the component C3, in full agreement with the experiment. The large anisotropy indicates that the orbital moment of C4 iron ions is relatively large, and this in turn leads to a larger sensitivity to the lattice defects. Substitution of Zn^{2+} for Fe^{3+} on the A site may be regarded as a "charged defect," which is likely to induce a notable change of the electronic structure of neighboring Fe ions on the B sites, a fact suggested also by the simultaneous change of B_{eff} and V_{zz} for C4. Note that low B_{eff} seems to be characteristic of the trimeron structure since for the atomic/electronic arrangement proposed by Patterson [3], where trimerons were not found, hyperfine magnetic fields for B7, B13, and B16 were higher.

Low B_{eff} components are easily seen in our Mössbauer data for $x = 0$ and 0.005, i.e., for first-order samples, and they are almost identical; this is a reliable result of our analysis. Since doping affects more orbital order than charge separation [21], it also suggests that the low B_{eff} is primarily the effect of charge disproportionation.

In the case of $x = 0.03$, the spectrum is different and the data treatment proposed in [5] does not result in a good fit (also the high-temperature results for $x = 0.03$ cannot be treated in the same way as for first-order samples; see below). Here also the line intensities for each component are not 3:2:1 as for other samples. The most straightforward option to

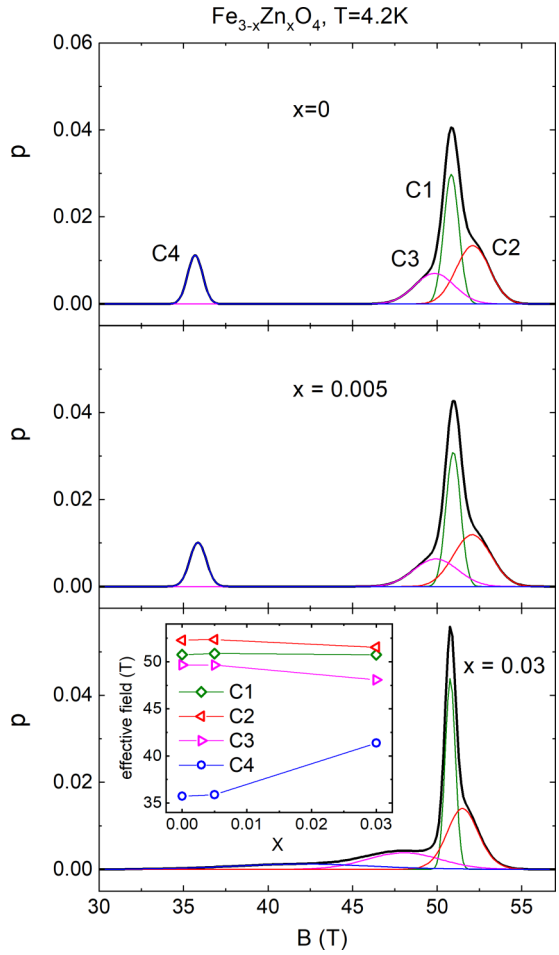

FIG. 4. Hyperfine field distribution p for all samples at $T = 4.2$ K as results from Voigt-function-based magnetic splitting distribution [18,19]. B_{eff} as a function of Zn content x is shown in the inset of a lower panel. The components are labeled as in Fig. 3.

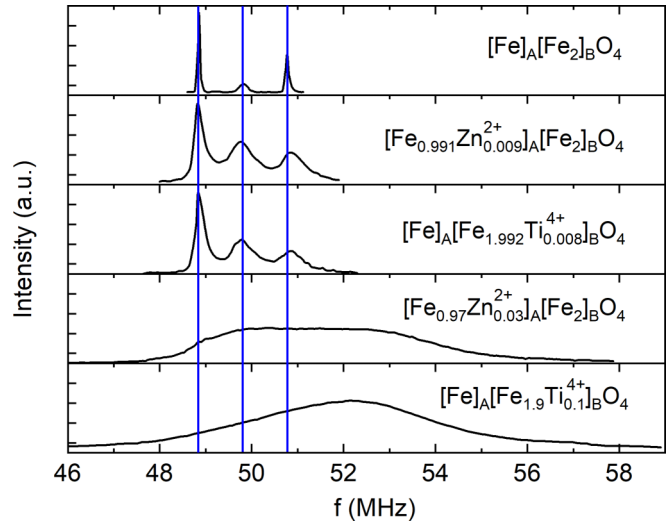

FIG. 5. ^{57}Fe NMR spectra of magnetite at $T = 4.2$ K with various types of defects; only the low-frequency part of the spectra is presented. Clearly resolved lines exist in the first-order regime (in Mössbauer spectra those lines are indistinguishable, and only one line is observed), while in second-order samples (both Zn-doped and Ti-doped), lines coalesce into a bump with the center of gravity moved to higher values, as in Mössbauer spectra (after [23], Fig. 7.19).

improve the fit is to increase the number of components. However, this is rather speculative as alternative options may be proposed with a similar increase of the fit quality. Therefore, in Figs. 4S and 5S of the supplemental material, the sample fit with five components at $T = 4.2$ K and the temperature dependence of hyperfine parameters drawn from these fits are presented, while the results of the same model as for first-order samples are shown here [Figs. 2(c) and 3]. The analysis shows that two components, one due to tetrahedral positions and the other coming from 3+-like octahedral sites, are very similar to those in first-order samples, but the other two components are largely affected. All these effects are best seen in Fig. 4, where an effective field distribution is presented (and the B_{eff} dependence on x is shown in the inset). In particular, the low-field component is smeared over a broad field range, and the center of gravity for sextet C3 (2+-like B sites) is slightly shifted to lower-field values, as compared to other samples. Also (see Fig. 3), the electric field gradient for this component is slightly lower than for the first-order samples, suggesting more symmetric surroundings.

The same results concerning B_{eff} were observed by Haley [22]: in powder stoichiometric magnetite, fitted with five components, the low B_{eff} component was present, while non-stoichiometric magnetite was fitted with three components and no traces of the low-field component were found.

Similar Zn-doped magnetite single crystals were measured by NMR. The results [23], reproduced here in Fig. 5, reveal three low-field B lines for stoichiometric samples, and for $x = 0.009$, while for $x = 0.03$ the lines are strongly broadened, forming a band rather than separated lines, with their center of gravity shifted to higher fields. This is likely to be connected to the above-mentioned sensitivity to the Zn substitution. Note that qualitatively similar features are observed in Ti-doped samples, despite the fact that 2+ valent Zn enters A iron positions, while tetravalent Ti resides in B sites. In these studies, the relative intensity of the "low-field part" with respect to "high-field lines" was not well-defined.

Thus, both in Mössbauer and NMR results there is a pronounced difference of low-T spectra between first-order and second-order samples with a very well seen change of a mean B_{eff} to higher values.

Since both our DFT analysis from [5] and DFT calculations in [3] showed that B_{eff} is sufficiently low only with a trimeron structure, trimerons may not exist in Zn-doped magnetite exhibiting a second-order Verwey transition, at least in its literal form described in [2]. We thus think that the low B_{eff} component is not Cc structure specific, as suggested in [24], but instead may be a fingerprint of magnetite of a first-order Verwey transition. The alternative is that Zn content gradually changes the electronic state of trimerons simply by slightly changing the valence of B iron. However, the drastic change of heat capacity (Fig. 1) and T_V versus x (Fig. 1S of the supplemental material) points to discontinuous rather than

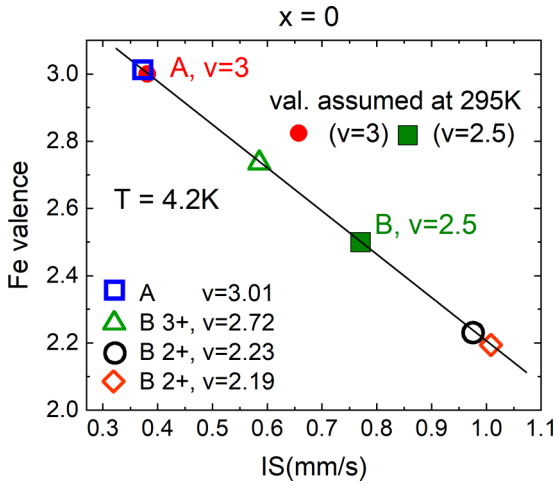

FIG. 6. Fe valences at $T = 4.2$ K as drawn from 295 K spectra of stoichiometric magnetite pinned, after correction for SOD, as 3+ (A sites) and 2.5+ (B sites) shown as bulk symbols.

gradual trimeron state alterations. Whatever the reason for the $x = 0.03$ sample being different from other specimens, the low-temperature structure of magnetite, either doped or nonstoichiometric, representing first- and second-order Verwey transitions, should be measured as thoroughly as was done in [2] and [21], and the presence of trimerons should be confirmed.

From the shape of the outermost lines (Fig. 3S [8]) and the temperature dependence of the hyperfine parameters shown in Fig. 3, it is clear that for all samples, IS and $B_{\rm eff}$, and to a lesser extent also V_{zz}, for the A component go practically smoothly across T_V from high to low temperatures [25]. This supports the long-lasting belief that tetrahedral positions and their electronic states do not change much when T drops below T_V, while real changes occur on octahedral iron sites. In fact, the Fe(A) nucleus is not the best probe to see the subtle reorganization of its surroundings because the dominant component to $B_{\rm eff}$ comes from the Fermi contact isotropic term [99.5% of the total magnetic field acting on Fe(A) [4]] reflecting the Fe(A) electronic state, not a magnetic field caused by Fe(B) ions (next nearest neighbors). Also, the spin-only Fe^{3+} state is basically isotropic (low V_{zz}), and a slight alteration of nearest-neighbor oxygen atoms at T_V is barely observed (Fig. 3). Taking all these into account, we can attribute IS for the Fe(A) component in the $x = 0$ sample (at 295 K) as representing 3+ valence and IS values for the remaining components as typical for 2.5+. We may thus calibrate the valence versus IS relation and draw Fe valences for the low-T phase. This is shown in Fig. 6 while the results are contained in Table II. Valences obtained in this way are close to those suggested in [2].

B. $T > T_V$

As seen from Figs. 3S [8] and 2 (aa, bb, and cc), the spectra at $T > T_V$ are similar, so initially the same fitting procedure was applied to all the samples. Three sextets were assumed: A iron position with relative intensity $I = 1$ and two components for B positions, with 1.5 (higher $B_{\rm eff}$) and 0.5 intensities.

This procedure worked well for first-order samples, and the hyperfine parameters drawn from it were presented in Fig. 3 (left and central panels). However, in the case of $x = 0.03$, the three-component fitting gave worse results. Also, some features seen in the low-T 72 K spectrum seem to be present, although in gradually decreasing extent, even at 295 K (e.g., hyperfine parameter distribution gets narrower upon heating). Lifting the 3:1 constraint resulted in only very limited improvement of the fit, while significantly better agreement was achieved when four components were assumed. However, as in case of the low-T phase, adding an additional component is speculative, not based on solid grounds. For this reason, the results of a sample fitting with three components, as for other samples, are presented in Fig. 3. In this case, to account for definitely wider parameter uncertainty, Voigt lines with Gaussian hyperfine field distributions were assumed to describe each component. This procedure was additionally justified by the broadened NMR lines of similar samples [28]. For comparison, fitting with four components is shown in Figs. 4Sb and 5S of the supplemental material.

The fact that neither low- nor high-T spectra for $x = 0.03$ can be satisfactorily fitted using the same model as for low-doped magnetite and that $B_{\rm eff}$ changes with x, as shown in Fig. 4, does not prove that Zn dopant with $x = 0.03$ causes a discontinuous effect on the electronic system. However, we think that the electronic effects caused by $x = 0.03$ Zn substitution are beyond the apparent geometrical effect such a substitution can cause, and they strongly suggest a discontinuous change of the electronic structure. A Zn atom replaces Fe(A) atoms, and with $x = 0.03$ statistically one Zn atom enters a single Cc unit cell. This means that 12 Fe(B) next nearest neighbors of the Zn atom are affected. However, the Fe(B)-Zn distance is about 3.48 Å [29] (in comparison to 1.88 Å of the O-Zn distance), and from the total of 18 atoms within this range around Fe(B) (six oxygen anions, six A-site cations, and six B-site cations), only one is Zn. Such simple geometrical arguments explain satellite NMR signals [28], but they do not seem to justify the effects we see in the Mössbauer spectrum and the large broadening of NMR Fe(B) lines of samples with a comparable amount of substitution [23]. Also, since for $x = 0.03$ magnetization still points along $\langle 111 \rangle$ [30] and thus approximately a 3:1 B-site division should still exist, we suspect that some major alteration of electronic structure must have discontinuously occurred, possibly linked, at $T > T_V$, to breaking Fd-$3m$ symmetry.

Our x-ray scattering experiment in ESRF on $Fe_{3(1-\delta)}O_4$ with $3\delta = 0.0162$ (second-order Verwey transition) was aimed at checking this conjecture. Although not the same crystal was used as for Mössbauer spectroscopy measurements, virtually all the properties that we have measured so far look the same for Zn- and Ti-doped and nonstoichiometric magnetite provided the properties for $x = 3\delta$ are compared, so we may safely assume that the same would be observed also for Zn-doped magnetite.

The main results of measurements, i.e., two high-symmetry cuts of reciprocal space, are presented in Fig. 7. Already at room temperature, the space group differs from Fd-$3m$, as no regular absences are observed. Moreover, we can anticipate short-range inhomogeneity from the deformed shape of

TABLE II. Mean Fe valences at $T = 4.2$ K, as well as charge per formula unit carried by Fe atoms, as drawn from IS after iron valences at 295 K were pinned as 3 (A positions) and 2.5 (B positions). IS at 295 K were adjusted for second-order Doppler shift (SOD) [16] (see also the supplemental material) calculated based on Debye temperature = 550 K [26,27].

Component	$x = 0$	$x = 0.005$	$x = 0.03$
comp. 1, $I = 8$ (7.76 for $x = 0.03$), A	$Fe^{3.01,}$ char = 3.01	$Fe^{3.00,}$ char = 3.0	$Fe^{3.01,}$ char = 2.92
comp. 2, $I = 8$, B 3+,	$Fe^{2.72,}$ char = 2.72	$Fe^{2.73,}$ char = 2.73	$Fe^{2.73,}$ char = 2.73
comp. 3, $I = 5$, B 2+,	$Fe^{2.23,}$ char = 1.39	$Fe^{2.22,}$ char = 1.39	$Fe^{2.31,}$ char = 1.44
comp. 4, $I = 3$, B 2+,	$Fe^{2.19,}$ char = 0.821	$Fe^{2.16,}$ char = 0.81	$Fe^{2.15,}$ char = 0.806
O charge = 8	Fe charge = 7.94	Fe charge = 7.93	Fe charge = 7.90

diffuse scattering in the proximity of Bragg reflections (closeup on the left panel).

Short-range correlations reflected by diffuse scattering were already found to be a result of electronic order below T_V [31] that survives, in some form, to room temperature. Our results show that some low-T electronic arrangement, whether or not it strictly resembles the trimeron structure described in [2], survives also in second-order nonstoichiometric magnetite, but within lower than Fd-3m crystal symmetry.

Diffuse scattering and how it depends on temperature were observed previously by neutron studies [32–34] and by anomalous x-ray diffraction [35]. For both types of magnetite, diffuse scattering increased upon cooling above T_V, but it abruptly diminished below T_V for first-order magnetite while continuing to increase for materials with a continuous Verwey transition. Since we have proved [12] that the lattice dynamics is very similar for both types of materials, and taking into account our heat capacity data [11], we repeat here that these are electronic arrangements that are different for both classes of materials below T_V.

Namely, the electron configuration pertaining to the trimeron structure, and resulting in low B_{eff} for first-order samples, is rigid: no excitation to the higher energy level is possible (low heat capacity) at $T < T_V$. When the thermal fluctuations of the lattice are sufficiently large, the excitation of the electronic system begins, resulting in the breakdown of Cc symmetry and further alteration of the electronic system (i.e., Verwey phase transformation). However, some short-range charge correlations, possibly trimeron-like, survive above T_V and show up in the form of diffuse scattering up to room temperature [31]. But in this high-T region, the low-T fingerprint of the "first-order" magnetite is lost: neither NMR nor the Mössbauer spectrum show low B_{eff}. Since the trimeron structure, i.e., that of the low-T phase, seems to be necessary for low B_{eff}, we think that a dynamic trimeron-like electronic arrangement, although existing in some form at $T > T_V$, is either not observed by slow Mössbauer/NMR techniques, or is altered by lattice symmetry change to Fd-3m and is different from that at low T.

In second-order samples, the ground state may also be trimeron-like, but with short-range inhomogeneity signaled by diffuse scattering [34]. This is due to many low-lying electronic energy states that can be excited already from lowest temperatures, 0.3 K [10], causing larger specific heat at $T_V < 125$ K. These excited electronic arrangements break the subtle partial cancelation of effective field components, which results in the lowest B_{eff} increasing. Note that this lower field is, to some extent, still present at $T = 4.2$ K (see Fig. 3, right panel), but it disappears at higher temperatures when the higher-level occupancy increases. One of those excited levels of the whole system has both different electronic as well as crystal order, and when fluctuation to this state increases, this level reorganizes and its energy becomes lower: this is the Verwey transition of the second-order magnetite.

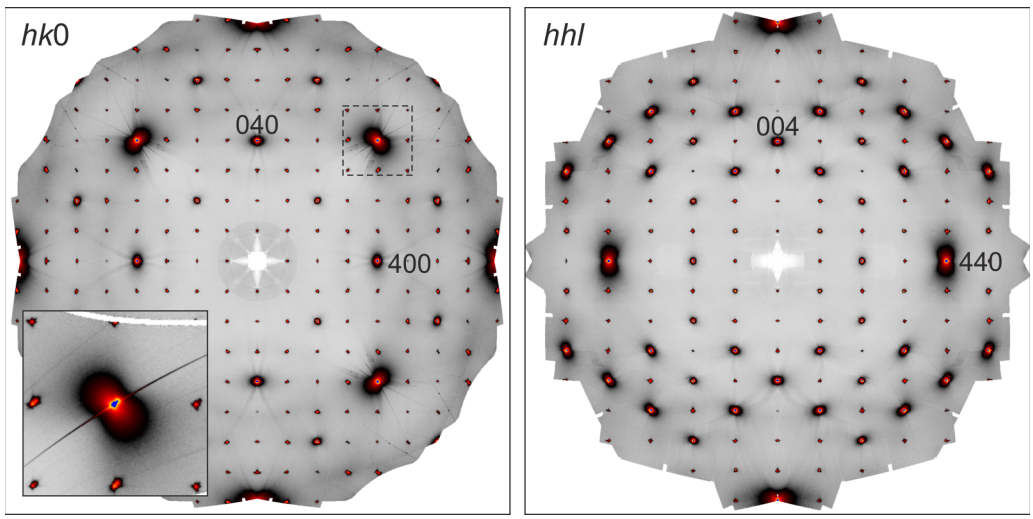

FIG. 7. Reciprocal space sections $hk0$ and hhl for $Fe_{3(1-\delta)}O_4$ with $3\delta = 0.0162$ measured at 295 K. Cubic Laue symmetry was applied in order to remove the detector gaps. The closeup on the left panel corresponds to the region defined by a dashed line.

Not only low T, but also high $T > T_V$ Mössbauer spectra for $x = 0.03$ are constantly changing with temperature. Thus, either further excitation to higher electronic levels within the symmetry other than Fd-3m is taking place, or the system is under continuous change of crystal/electronic structure.

Naturally, this scenario needs thorough confirmation. First, precise crystal lattice studies should be performed at $T < T_V$ for $x > 0.012$ since we postulate that other electronic levels, higher than a trimeron-like electronic arrangement, are already occupied, thus the structure will result from a mixture of many electronic states, not just trimerons. Also, additional Mössbauer as well as NMR measurements should be performed at the lowest available temperatures, below 4.2 K; we suspect that the low B_{eff} component will be visible at very low T, but it will disappear upon heating. Finally, precise measurements of high-temperature $T > T_V$ structure studies should be carried out on doped samples to find the crystal structure and to determine at what concentration of dopant it departs from Fd-3m. In fact, also our DFT calculations, when confined to cubic structure, depart from Fd-3m to some other atomic cubic arrangements of lower symmetry. This suggests that high-T structure is a dynamic mixture of several cubic phases, fast enough to average out to Fd-3m in first-order samples, but too slow in the case of more doped materials, thus showing up as lower than Fd-3m symmetry at the timescale of the x-ray scattering experiment.

DFT calculations of the electronic structure for Zn-doped magnetite would be highly desirable. They will be rather demanding, however, particularly in the low-temperature crystal structure for which only identity remains as a symmetry operation. Moreover, the results may depend on the site in which Fe is replaced by Zn. Despite these obstacles, we plan to perform and analyze such calculations in the near future.

IV. CONCLUSIONS

Our aim was to use a microscopic technique, namely Mössbauer spectroscopy, to observe the difference between samples exhibiting "first-" and "second-order" Verwey transitions, very easily reflected by bulk techniques such as, e.g., heat capacity. We measured three single crystalline magnetite samples (stoichiometric and two Zn-doped) with (001) orientation along incoming gamma rays.

Very similar Mössbauer spectra were observed for first-order magnetite samples (stoichiometric and with $x = 0.005$), but different in the case of second order ($x = 0.03$), where also the continuous change with temperature, both at $T < T_V$ and above T_V, was found. Our analysis of low-T Mössbauer data, supported by the results of DFT calculations for stoichiometric magnetite electronic structure [5], showed similar hyperfine parameters for first-order samples, but different for the second order; in particular, the low $B_{\text{eff}} = 36\,\text{T}$ component, characteristic for a trimeron-like electronic arrangement, is shifted to higher fields and considerably broadened if not missing at all. This suggests that this low B_{eff} may be treated as a fingerprint of a first-order magnetite trimeron lattice arrangement that does not survive, at least in this literal form, up to high $T > T_V$, despite the presence of some electronic arrangement up to room temperature [31]. We have also found that imposing three components for the fit of the high-T Mössbauer spectrum for the second-order sample gave lower quality fits than for first-order samples. This coincides with the results of our synchrotron crystal structure observation of nonstoichiometric, second-order single crystal that showed lower than Fd-3m symmetry. All those findings call for precise structural studies of doped/nonstoichiometric magnetite.

[1] F. Walz, J. Phys.: Condens. Matter **14**, R285 (2002).

[2] M. S. Senn, J. P. Wright, and J. P. Attfield, Nature (London) **481**, 173 (2012); M. S. Senn, I. Loa, J. P. Wright, and J. P. Attfield, Phys. Rev. B **85**, 125119 (2012).

[3] C. H. Patterson, Phys. Rev. B **90**, 075134 (2014).

[4] R Řezníček, V. Chlan, H. Štěpánková, and P. Novák, Phys. Rev. B **91**, 125134 (2015).

[5] R. Řezníček, V. Chlan, H. Štěpánková, P. Novák, J. Żukrowski, A. Kozłowski, Z. Kąkol, Z. Tarnawski, and J. M. Honig, Phys. Rev. B **96**, 195124 (2017).

[6] Although the properties of stoichiometric and low-doped magnetite from one side and those more heavily doped (but below 1% for Zn, Ti, and the nonstoichiometry level) from the other are definitely different and, therefore, these two classes of magnetite samples are frequently dubbed "magnetite of first- and second-order Verwey transition," this description is not fully justified in a strict thermodynamic sense. First, the presence of latent heat, which is the prerequisite of a discontinuous transition, cannot be confirmed definitively in doped samples, apart from the stoichiometric and very slightly oxidized ones. Second, no appreciable hysteresis exists (beyond 0.03 K [7]) in slightly doped samples, while in samples from a the higher dopand/nonstoichiometry region clear hysteresis occurs, which the authors experienced several times and is shown in [9]. To the best of our knowledge, these problems in magnetite were never pursued further. Having all these in mind, we nevertheless decided to use the notion "magnetite of first and second character" as a shortcut for a more complicated situation.

[7] Z. Tarnawski, A. Wiecheć, M. Madej, D. Nowak, D. Owoc, G. Król, Z. Kąkol, L. Kolwicz-Chodak, A. Kozłowski, and T. Dawid, Acta Phys. Pol. A **106**, 771 (2004).

[8] See Supplemental Material at http://link.aps.org/supplemental/10.1103/PhysRevB.98.125138 for additional figures, sample preparation, and check, and for Mössbauer experiment details. The Supplemental Material includes Refs. [16,26,27,36–39].

[9] R. Aragón, R. J. Rasmussen, J. P. Shepherd, J. W. Koenitzer, and J. M. Honig, J. Magn. Magn. Mater. **54–57**, 1335 (1986).

[10] J. W. Koenitzer, P. H. Keesom, and J. M. Honig, Phys. Rev. B **39**, 6231 (1989).

[11] A. Kozłowski, Z. Kąkol, D. Kim, R. Zalecki, and J. M. Honig, Phys. Rev. B **54**, 12093 (1996).

[12] T. Kołodziej, A. Kozłowski, P. Piekarz, W. Tabiś, Z. Kąkol, M. Zając, Z. Tarnawski, J. M. Honig, A. M. Oleś, and K. Parliński, Phys. Rev. B **85**, 104301 (2012).

[13] H. R. Harrison and R. Aragón, Mater. Res. Bull. **13**, 1097 (1978).

[14] R. Aragón, H. R. Harrison, R. H. McCallister, and C. J. Sandberg, J. Cryst. Growth **61**, 221 (1983).

[15] H. Flood and D. G. Hill, Z. Elektrochem. **61**, 18 (1957).

[16] N. N. Greenwood and T. C. Gibb, *Mössbauer Spectroscopy* (Chapman and Hall, London, 1971); P. Gütlich, R. Link, and A. Trautwein, *Mössbauer Spectroscopy and Transition Metal Chemistry* (Springer, Berlin, 1978).
[17] In all figures and the text below, the phrase "isomer shift" (IS) stands for the center of the spectrum component shift. This shift is affected by the real isomer shift, the parameter calculated in [5], and the temperature-dependent second-order Doppler shift.
[18] D. G. Rancourt, Nucl. Instrum. Methods B **44**, 199 (1989).
[19] D. G. Rancourt and J. Y. Ping, Nucl. Instrum. Methods B **58**, 85 (1991).
[20] http://www.rigaku.com/en/products/smc/crysalis.
[21] G. Perversi, J. Cumby, E. Pachoud, J. P. Wright, and J. P. Attfield, Chem. Commun. **52**, 4864 (2016).
[22] G. Haley, J. G. Mullen, and J. M. Honig, Solid State Commun. **69**, 285 (1989).
[23] R. Řezníček, Ph.D. thesis, Charles University, Prague, 2015.
[24] M. P. Pasternak, W. M. Xu, G. Kh. Rozenberg, R. D. Taylor, and R. Jeanloz, J. Magn. Magn. Mater. **265**, L107 (2003).
[25] Although a small step is apparent in the temperature dependence of frequency of NMR Fe(A) line (center of gravity below T_V) in pure magnetite [28].
[26] E. F. Westrum and F. Gronveld, The J. Chem. Therm. **1**, 543 (1969).
[27] N. W. Grimes, Philos. Mag. **26**, 1217 (1972).
[28] R. Řezníček, H. Štěpánková, V. Chlan, P. Novák, and A. Kozłowski, IEEE Trans. Magn. **48**, 3039 (2012).
[29] Z. Kąkol, D. Owoc, J. Przewoźnik, M. Sikora, C. Kapusta, D. Zając, A. Kozłowski, J. Sabol, and J. M. Honig, J. Solid State Chem. **192**, 120 (2012).
[30] J. W. Koenitzer, Ph.D. thesis, Purdue University, 1992.
[31] A. Bosak, D. Chernyshov, M. Hoesch, P. Piekarz, M. Le Tacon, M. Krisch, A. Kozłowski, A. M. Oleś, and K. Parlinski, Phys. Rev. X **4**, 011040 (2014).
[32] Y. Fujii, G. Shirane, and Y. Yamada, Phys. Rev. B **11**, 2036 (1975).
[33] S. M. Shapiro, M. Iizumi, and G. Shirane, Phys. Rev. B **14**, 200 (1976).
[34] R. Aragón, P. M. Gehring, and S. M. Shapiro, Phys. Rev. Lett. **70**, 1635 (1993).
[35] T. Toyoda, S. Sasaki, and M. Tanaka, Jpn. J. Appl. Phys. **36**, 2247 (1997).
[36] M. Bałanda, A. Wiecheć, D. Kim, Z. Kąkol, A. Kozłowski, P. Niedziela, J. Sabol, Z. Tarnawski, and J. M. Honig, Eur. Phys. J. B **43**, 201 (2005).
[37] W. Tabiś *et al.*, J. Phys. Condens Matter **25**, 055603 (2013).
[38] R. S. Coe, R. Egli, S. A. Gilder, and J. P. Wright, Earth Planet. Sci. Lett. **319**, 207 (2012).
[39] S. Margulies and J. R. Ehrman, Nucl. Instrum. Methods **12**, 131 (1961); G. K. Shenoy, J. M. Friedt, H. Maletta, and S. L. Ruby, in *Mössbauer Effect Methodology*, edited by I. J. Gruverman, C. W. Seidel, and D. K. Dieterly (Plenum, New York, 1974), Vol. 10, p. 277.